

We are IntechOpen, the world's leading publisher of Open Access books Built by scientists, for scientists

4,800

Open access books available

122,000

International authors and editors

135M

Downloads

Our authors are among the

154

Countries delivered to

TOP 1%

most cited scientists

12.2%

Contributors from top 500 universities



WEB OF SCIENCE™

Selection of our books indexed in the Book Citation Index
in Web of Science™ Core Collection (BKCI)

Interested in publishing with us?
Contact book.department@intechopen.com

Numbers displayed above are based on latest data collected.

For more information visit www.intechopen.com



Efficient Sensorless PMSM Drive for Electric Vehicle Traction Systems

Driss Yousfi, Abdelhadi Elbacha and Abdellah Ait Ouahman
*Cadi Ayyad University, ENSA-Marrakech
Morocco*

1. Introduction

With ever increasing oil prices and concerns for the natural environment, there is a fast growing interest in electric vehicles (EVs). However, energy storage is the weak point of the EVs that delays their progress. For this reason, a need arises to build more efficient, light weight, and compact electric propulsion systems, so as to maximize driving range per charge. There are basically two ways to achieve high power density and high efficiency drives. The first technique is to employ high-speed motors, so that motor volume and weight are greatly reduced for the same rated output power. However, mechanical losses are incurred by the clutch, reduction and differential gears, during power transmission from the motor to the wheels. With such driveline transmission, losses amount up to 20% of the total power generated (Jain & Williamson, 2009).

A more attractive solution involves employing high-torque, low-speed motors (around 1000rpm); which can be directly mounted inside the wheel, known as in-wheel motors or hub motors. By applying wheel motors in EVs, power transmission equipment can be eliminated. Therefore, transmission losses are minimized and operating efficiency is improved (Chau et al., 2008).

The basic requirements of wheel motors are large starting torque, overload capability, wide speed range, and high power density in order to reduce motor weight. A low motor weight is essential when the motor is fitted inside the wheel to reduce un-sprung mass, thus maintaining the quality of road holding. Hence, high efficiency/weight ratio is required for a wheel motor.

Considering these requirements, several types of motors have been reported in literature for use as an in-wheel motor: Induction motor, Permanent Magnet Brushless motor and switched reluctance motor (Emadi, 2005; Jain & Williamson, 2009). Amongst these solutions, PM Brushless motors might play a major role in the future development of in-wheel applications, because of its high power density and efficiency, smooth torque, and simple control drive.

The PM Brushless motor has either a trapezoidal-wave or a sine-wave Back-EMF. In the trapezoidal-wave motor, cheap Hall-effect sensors are used to control commutation. The interaction between the fed trapezoidal-wave current and magnetic field, produces more frequency harmonics and a larger torque ripple. In the PM Brushless motor with sinusoidal Back-EMF a continuous rotor position sensor is indispensable. In addition to commutation purposes, this measurement is used to eliminate the problems associated with the

trapezoidal-wave version. Because these types of sensors are expensive and cumbersome, a number of position measurement elimination techniques have been reported to operate such motors with sensorless strategies. When reviewing papers published in this field i.e. sensorless control applied to wheel motors, it is evident that there has not been so many published contrary to other industrial applications.

Some of reported rotor position estimation techniques are based on the vector control principle of AC motors (Chen, et al., 2010; Genduso et al., 2010; Jingbo, et al., 2010). The state estimation algorithms, such as a state observer or an extended Kalman filter, are also adopted to estimate the rotor position and the speed (Batzel & Lee, 2005). Other rotor position estimation techniques reported in (Carpaneto, et al., 2009; Cheng & Tzou, 2003; Johnson, et al., 1999; Sungyoon, et al., 2010; Yousfi, 2009) are based on the flux linkages, which can be obtained from the stator voltages and the currents of the motors. The flux linkage based methods operate accurately over a wide speed range and can be applied to the PM Brushless motors with either trapezoidal or sinusoidal Back-EMFs. However, the performance of the position estimation depends very much on the quality and the accuracy of the estimated flux linkages.

In all of these algorithms, extensive computational power and accurate measurement of the voltages and currents, as well as accurate knowledge of the motor parameters are required. Moreover, the methods proposed so far ultimately fail at low and zero speed in wheel motor tests due to the absence of measurable signals. Indeed, the position error and the torque losses are relatively large in these conditions.

From the mathematical model of the PM Brushless Motor, it can be observed that the Back-EMF or flux linkage varies as a function of the rotor position. Therefore, if these quantities are measured or estimated, the rotor position information can be determined. However, it is difficult to measure the Back-EMFs, specifically at low operating speeds, or the flux linkages directly because of the integration drift and/or shift.

To solve the aforementioned position estimation problems, this chapter presents a direct algebraic calculation method of the flux linkage, instead of the Back-EMF integration. Hence, sensorless vector control of the PM Brushless Motor could be applied in order to raise the efficiency of the drive. During the initial operation, the motor is started up using the Hall-effect signals to develop the required high starting torque.

2. PM Brushless motor commutation

In many EV applications, PM Brushless in-wheel Motor is preferred for its high efficiency. In such configuration, the motor is integrated in the wheel in order to eliminate transmission losses and simplify the mechanical design. A basic EV system with in-wheel motors is shown in Fig.1.

2.1 Brushless motor types

There are two main types of Brushless motors (Gieras et al., 2004; Hanselman, 2006 ; Krishnan, 2010). One is known as the Brushless DC Motor (BLDCM), characterized by constant flux density in the air gap around the pole faces. The motor windings should be supplied with currents in the form of rectangular pulses.

The other motor ideally has sinusoidal flux and sinusoidal distribution of its windings. It is supplied with a sinusoidal current and is known as the Permanent Magnet Synchronous Motor (PMSM).

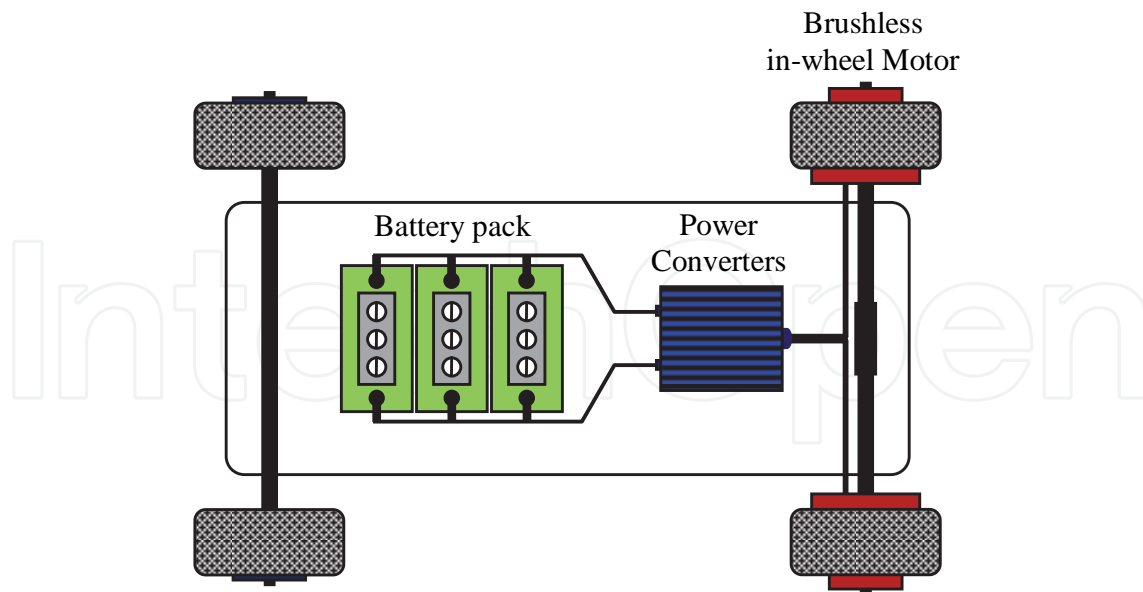


Fig. 1. Schematic of an Electric Vehicle with in-wheel motors.

The commutation process has to ensure that the action of switching the current direction is synchronized with the movement of the flux in the air gap, and so the motor must have a sensor for measuring the position of the flux wave relative to that of the stator windings. Simple Hall-effect sensors are used with BLDCM in order to manage the commutation sequence and form the appropriate current waveform. On the other hand, a high resolution encoder or resolver is necessary for the PMSM control mode to generate sinusoidal currents.

2.2 Current and torque waveforms

Fig. 2 shows experimental currents and torques for the same motor used in BLDCM (120° commutation) and PMSM control modes under the same operating conditions. By driving the motor with rectangular current commutation, more frequency harmonics are present in the current waveform as shown in Fig. 2-a. That is reflected, at the level of the generated torque, as a relatively intense ripple at 6 times the fundamental frequency and weighing 13% of the rated torque. As a result, the ageing process of the motor is accelerated.

In the PMSM control mode (Fig. 2-b), these problems practically disappear and a larger torque is produced for the same RMS current. Thus, an immediate reduction in power losses occurs. The sinusoidally driven motor gains 7.5% in energy consumption compared to BLDC mode. Although this rate might be worthless in conventional electric drive applications, it is valuable in EV case where batteries are the only source of energy.

The smoothness of the PMSM output torque is only affected by the ripple in the flat top caused by stator slotting and the fringing effects. However, in BLDCM, further irregularities in the rotor output torque arise from stator current waveforms which are never perfectly rectangular in practice.

Most EV dedicated brushless hub motors come with Hall-effect sensors for BLDC control end. Unfortunately, PMSM control mode requires more precise angle measurements. Consequently, position and speed estimators would be an effective solution to carry out the PMSM control and benefit from its advantages, without using cumbersome mechanical sensors.

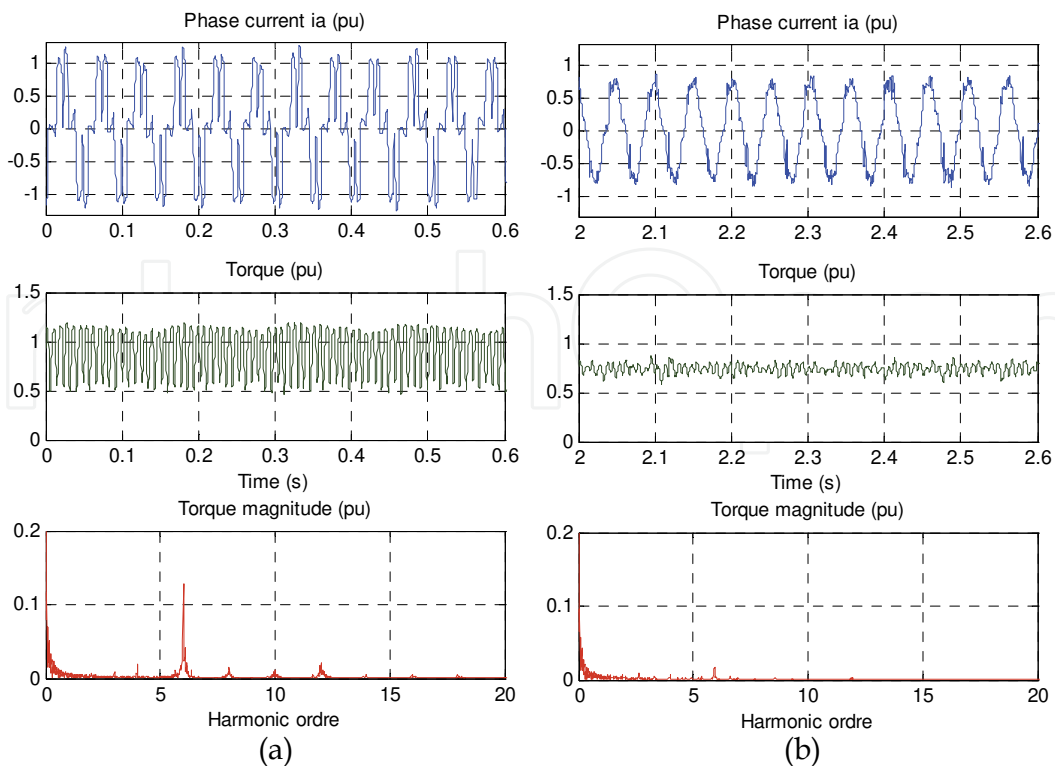


Fig. 2. Phase current, torque and torque spectrum at 50 rpm in (a) BLDCM and (b) PMSM control modes

3. Mathematical model of the motor

In this section, a brief description of the PMSM model is presented since the investigated estimation method needs to manipulate the equations of the machine. The model of the PMSM in the stationary frame (α - β) is:

$$\begin{aligned} v_{\alpha} &= Ri_{\alpha} + e_{\alpha} \\ v_{\beta} &= Ri_{\beta} + e_{\beta} \end{aligned} \quad (1)$$

$$\begin{aligned} e_{\alpha} &= \frac{d\psi_{\alpha}}{dt} \\ e_{\beta} &= \frac{d\psi_{\beta}}{dt} \end{aligned} \quad (2)$$

where $e_{\alpha\beta}$, $\psi_{\alpha\beta}$, $v_{\alpha\beta}$ and $i_{\alpha\beta}$ are respectively the Back-EMF, flux linkages, terminal voltages and phase currents in $\alpha\beta$ -frame, and R the winding resistance.

The flux linkages are generated in term of position as:

$$\begin{aligned} \psi_{\alpha} &= L_{\alpha}i_{\alpha} + \psi_m \cos\theta \\ \psi_{\beta} &= L_{\beta}i_{\beta} + \psi_m \sin\theta \end{aligned} \quad (3)$$

θ is the actual rotor angle.

ψ_m is the maximum flux linkage of the permanent magnet.

L_α, L_β are the inductances in $\alpha\beta$ -frame.

The used Brushless motor is a non-salient machine with sinusoidal Back-EMF. So the inductances in the model are equal i.e. $L_\alpha=L_\beta=L$.

The above electrical and magnetic equations are the basis for the position and speed extraction from the voltage and current measurement.

4. Position and speed estimation

In the PMSM operating mode, in order to generate smooth torque and thus reduce power losses, vibration and noise, the current waveform should match the shape of the sinusoidal motor Back-EMF. Consequently, high resolution rotor position feedback is of critical importance. On the other hand, speed feedback is required for accurate velocity tracking. Hence, in the absence of an optical encoder, suitable strategies must be developed to determine these parameters. Figure 3 illustrates a common vector control scheme with a position and speed estimator instead of an encoder.

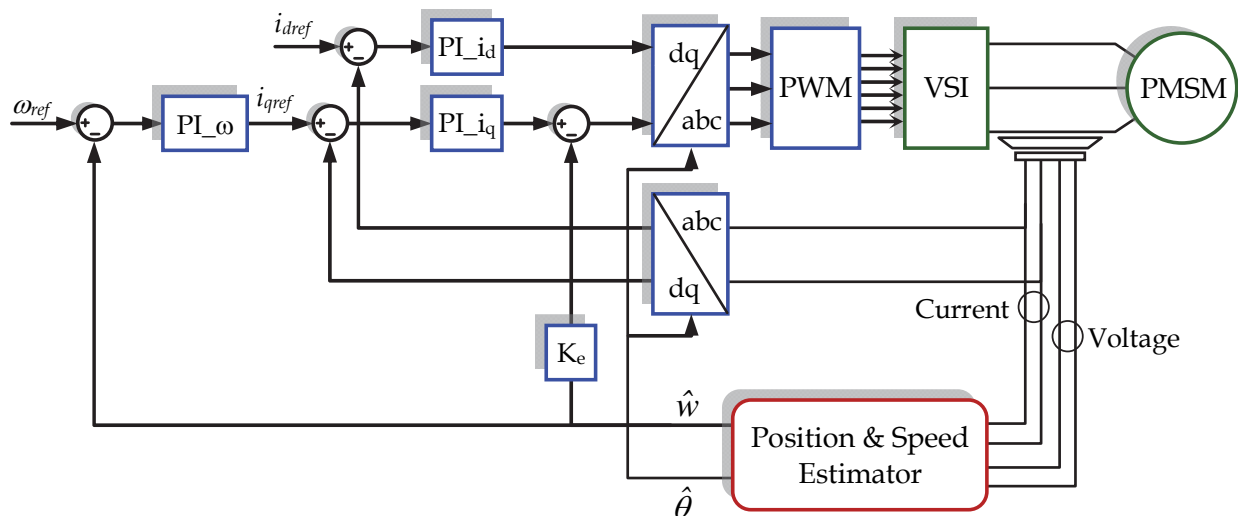


Fig. 3. PMSM sensorless vector control with position and speed estimator.

4.1 Rotor position estimation using hall-effect signals

Simple rotor position estimation can be obtained through direct digital signal processing of the Hall-effect sensor outputs (Johnson, et al., 1999; Morimoto et al., 1996). The electric angular position is generally given by:

$$\theta(t) = \int_{t_k}^t \omega(t) dt + \theta_k \tag{4}$$

$\omega(t)$ is the instantaneous electric angular velocity and θ_k is the initial angle of sector k measured from a fixed reference axis.

t_k is the instant when the magnetic axis enters sector k ($k=1, 2, \dots, 6$).

The zeroth-order position estimation algorithm is obtained by taking into account the zeroth-order term of an approximated Taylor series expansion.

The Hall-effect sensors detect when the rotor magnetic axis enters a 60° sector. Then, the speed can be expressed as the approximation:

$$\omega(t) \approx \hat{\omega}_{0k} = \frac{\pi / 3}{\Delta t_{k-1}} \quad (5)$$

Δt_{k-1} is the time interval taken by the rotor magnetic axis to cross the previous sector $k-1$.

The electric angular position can be obtained by numerical integration of (4), applying the constraint that the resulting angular position value has to be within sector k limits. The angular position is, thus, calculated as:

$$\begin{aligned} \hat{\theta}(t) &= \theta_k + \hat{\omega}_{0k} \times (t - t_k) \\ \text{with } \theta_k &\leq \hat{\theta}(t) \leq \theta_k + \pi/3 \end{aligned} \quad (6)$$

The position estimate can be also derived as a second-order algorithm by taking into account higher order terms of the Taylor series expansion.

The block diagram of this estimation technique is shown in Fig. 4.

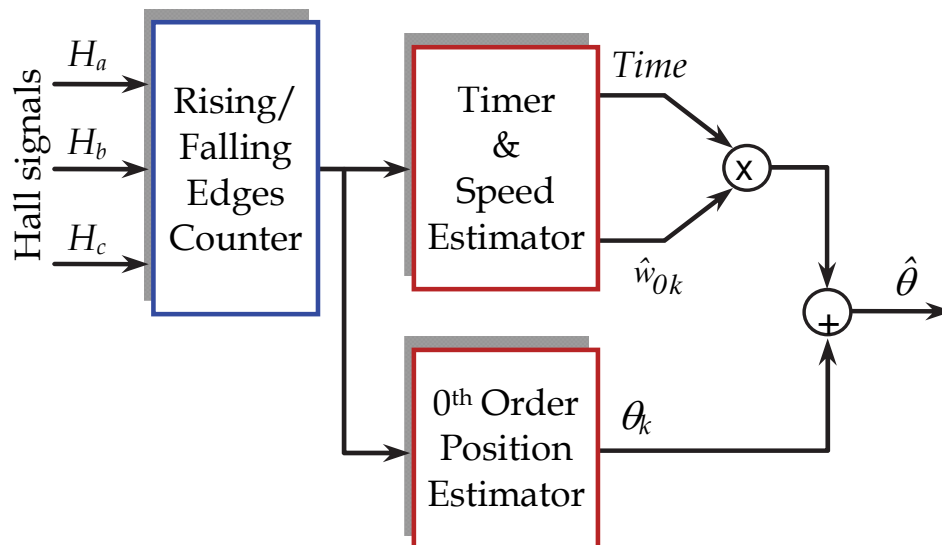


Fig. 4. Block diagram of the Hall-effect sensor based estimator.

The estimation here depends exclusively on the motor speed and the sampling time. So, more attention should be paid to the sampling time in high speed operation particularly. For the test motor, the frequency of the Hall signals goes beyond 1.4 kHz at rated speed; therefore relatively fast sampling time should be used for the estimation ($100 \mu\text{s}$).

The estimation weakness in this method intensifies during velocity transitions, as shown in Fig. 5. When the motor accelerates, the estimated position deviates from the real position between the Hall-effect signals. This is due to the error between the actual speed and the time based estimated speed from Hall sensors. Such a position error affects current regulation and degrades torque production.

Furthermore, the position estimation error is proportional to the rotor speed. Consequently, the estimation capability could entirely deteriorate when the speed becomes relatively high as in Fig. 6.

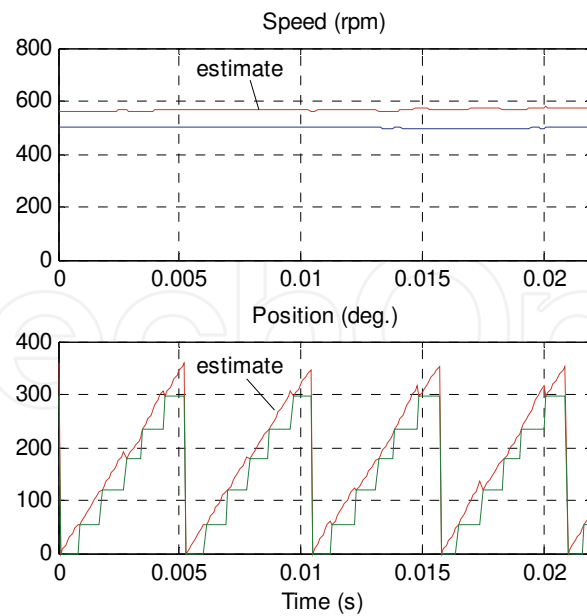


Fig. 5. Speed and 1st order position estimates deviation during motor acceleration around 500 rpm.

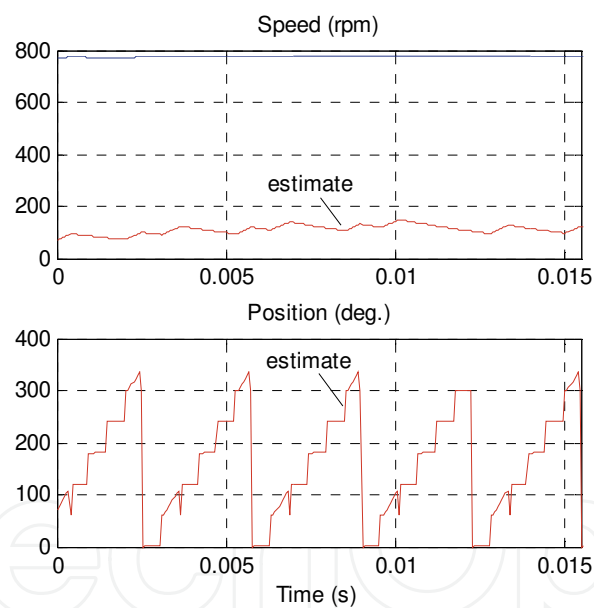


Fig. 6. Deterioration of the estimator at 780 rpm.

4.2 Back-EMF based rotor position estimator

The flux can be used to estimate the rotor angular position. Especially in steady-state, the actual flux linkage vector is synchronized to the rotor and the flux linkage vector position is the true rotor position.

However, because of the measurement imperfection which must be corrected by means of a filter, an error occurs in the phase angle and magnitude of the flux linkage estimation. This uncertainty depends on the speed, and it increases when the motor operates at a frequency lower than the filter cut-off frequency. A correction routine is set up for this reason.

Commonly, direct measurements of the line current and phase voltage allow estimation of the flux linkage through the well-known integration:

$$\begin{aligned}\psi_{\alpha} &= \int e_{\alpha} dt = \int (v_{\alpha} - Ri_{\alpha}) dt \\ \psi_{\beta} &= \int e_{\beta} dt = \int (v_{\beta} - Ri_{\beta}) dt\end{aligned}\quad (7)$$

From the estimation of ψ_{α} and ψ_{β} , the rotor angle estimate may be determined as:

$$\operatorname{tg} \theta = \frac{\sin \theta}{\cos \theta} = \frac{\psi_{\alpha} - Li_{\alpha}}{\psi_{\beta} - Li_{\beta}}\quad (8)$$

Thus

$$\hat{\theta} = \operatorname{arctg} \frac{\psi_{\alpha} - Li_{\alpha}}{\psi_{\beta} - Li_{\beta}}\quad (9)$$

At this stage a four-quadrant arctan function is used.

The integration of Eq. 7 by pure integrator involves drift and saturation problems. Since the integration at $t=0s$ time instant requires initial condition, the rotor must be brought to a known position. However, this prior setting is not possible in EV context.

To avoid the pure integrator and solve the problems, one can benefit from the fact that the flux ψ_{α} and ψ_{β} are respectively cosine and sine function of the position (Yousfi & El Adnani, 2007). They can be derived, immediately, from the Back-EMFs e_{α} and e_{β} by using the following algebraic calculation:

$$\begin{aligned}\psi_{\alpha} &= \frac{e_{\alpha}}{\omega} \\ \psi_{\beta} &= -\frac{e_{\beta}}{\omega}\end{aligned}\quad (10)$$

In this way, there is no need of position or flux linkage initial values.

In practice the Back-EMF measurement, used to evaluate the flux estimate, contains an offset which causes additional position errors. The solution consists of detecting this offset with a very low cut-off frequency LP Filter and subtracting it from the original signal.

4.3 Rotor speed estimation

It is clear from Eq. 10 that the rotor speed is required first for the implementation of the rotor position estimator. Eq. 1 can be used to extract the speed, since the Back-EMF magnitude E_m already contains this quantity:

$$e_{\alpha}^2 + e_{\beta}^2 = L^2 \left(\frac{di_{\alpha}}{dt}^2 + \frac{di_{\beta}}{dt}^2 \right) - 2LE_m \left(\frac{di_{\alpha}}{dt} \sin \theta - \frac{di_{\beta}}{dt} \cos \theta \right) + E_m^2\quad (11)$$

where

$$E_m = \omega \psi_m\quad (12)$$

Until the rated speed operation, the first term on the right hand of Eq. 11 stays below 5% of the overall magnitude because the motor inductance is very small. However, the second term reaches 45% near this speed and cannot be neglected.

Consequently, when the motor operates relatively far from the rated conditions the following approximation is valid:

$$e_{\alpha}^2 + e_{\beta}^2 \approx \omega^2 \psi_m^2 \quad (13)$$

This leads to a simple manner of estimating the speed magnitude:

$$|\hat{\omega}| \approx \frac{\sqrt{e_{\alpha}^2 + e_{\beta}^2}}{\delta \psi_m} \quad (14)$$

Here, δ is an adjustment coefficient introduced to compensate the neglected term in Eq. 11. The direction of the speed estimate at sampling interval kT_e is then obtained from the Back-EMF angle evolution, as follow:

$$\varphi(k) = \arctg\left(\frac{-e_{\alpha}(k)}{e_{\beta}(k)}\right) \quad (15)$$

$$\hat{\omega}(k) = \text{sgn}(\varphi(k) - \varphi(k-1)) |\hat{\omega}(k)| \quad (16)$$

The strength of this method is its ability to determine speed, even at low speed. The weakness is its dependence on motor parameters.

The above model based speed estimator may not be a good solution when the speed increases and approaches the rated value. A simpler manner of estimating the speed magnitude, at this speed range, is the derivation of the position estimate:

$$\hat{\omega} = \frac{d\hat{\theta}}{dt} \quad (17)$$

Obviously, the resulting speed needs to be Low-Pass filtered.

4.4 Position error correction

The open-loop structure of the position estimator that uses stator voltage and current measurement as well as speed-division, leads to cumulative position estimation error. In addition, the use of LP filters in the estimation line induces a phase shift, and thus, an additional error. The position error affects current regulation and degrades torque production. Based on the above considerations, a position correction procedure using Hall-effect signals, is implemented to compensate all sources of position estimation error.

It is important to note that the position estimation cannot be achieved near zero-speed when the electric measurements are weak and the speed-based division is unstable (Capponi et al., 2004; Yousfi, 2009).

For this reason, the motor is started up as a BLDC motor using Hall-effect signals until the rotor speed reaches convenient level for angle estimation.

Complete structure of the proposed position and speed estimator is presented in Fig. 7.

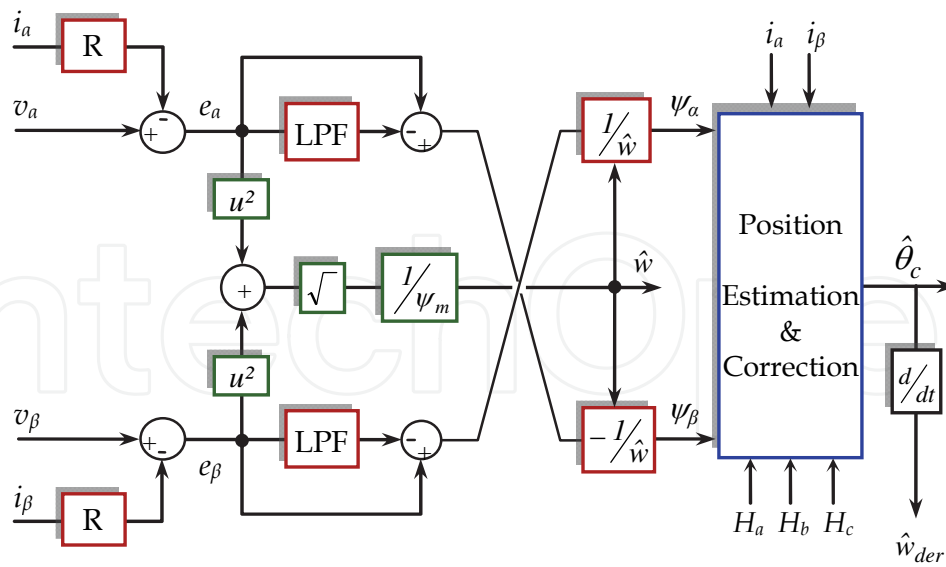


Fig. 7. Block diagram of the Back-EMF/Hall-effect based position and speed estimator.

This estimation method depends mainly on two machine parameters i.e. the winding resistance R and the inductance L . The second advantage of this method is its estimation capability even at low speed range and high load rate. In addition, thanks to the BLDC starting mode using Hall-effect sensors, high torque is possible at any initial moment.

5. Experimental setup and results

An experimental set up was fabricated in the laboratory using a 48V/2kW in-wheel gearless Brushless motor which is fed by a three-phase full bridge inverter built using compact Intelligent Power Module (IPM) (Fig. 8). This system is powered by 48V/75AH battery pack. For estimation and control tasks, an eZdsp2812 board has been used. To keep an eye on the control mode of the motor, the Park frame currents (d-q) are measured.



Fig. 8. Experimental setup for the in-wheel brushless motor drive validation and the IPM based power circuit.

In EV applications, current and voltage measurements are often required in order to carry out advanced motor control strategies, to estimate the position and speed of the machine or to carry out online energy management. In the current application, phase currents are provided by the LEM transducers used for the implementation of the motor vector control. On the other hand, an indirect voltage measurement that uses the PWM duty cycle and the DC bus voltage to estimate the inverter output voltage is used to reduce the drive sensors number. Thus, for each phase the voltages are reconstructed every sample period using the following method:

$$v = DV_{dc} - v_{comp} \tag{18}$$

V_{dc} is the DC Link voltage measured via LEM sensor that already exists for battery energy management purposes, and D is the PWM duty cycle.

The compensation term v_{comp} is associated with the inverter device losses and is determined from non-linear tables relating inverter device voltage drop to phase current.

The block diagram of the developed control scheme is shown in Fig. 9. Inputs to the position estimator are motor stator currents and voltages as well Hall sensor signals. The output is a high resolution estimate of the rotor position and speed estimation.

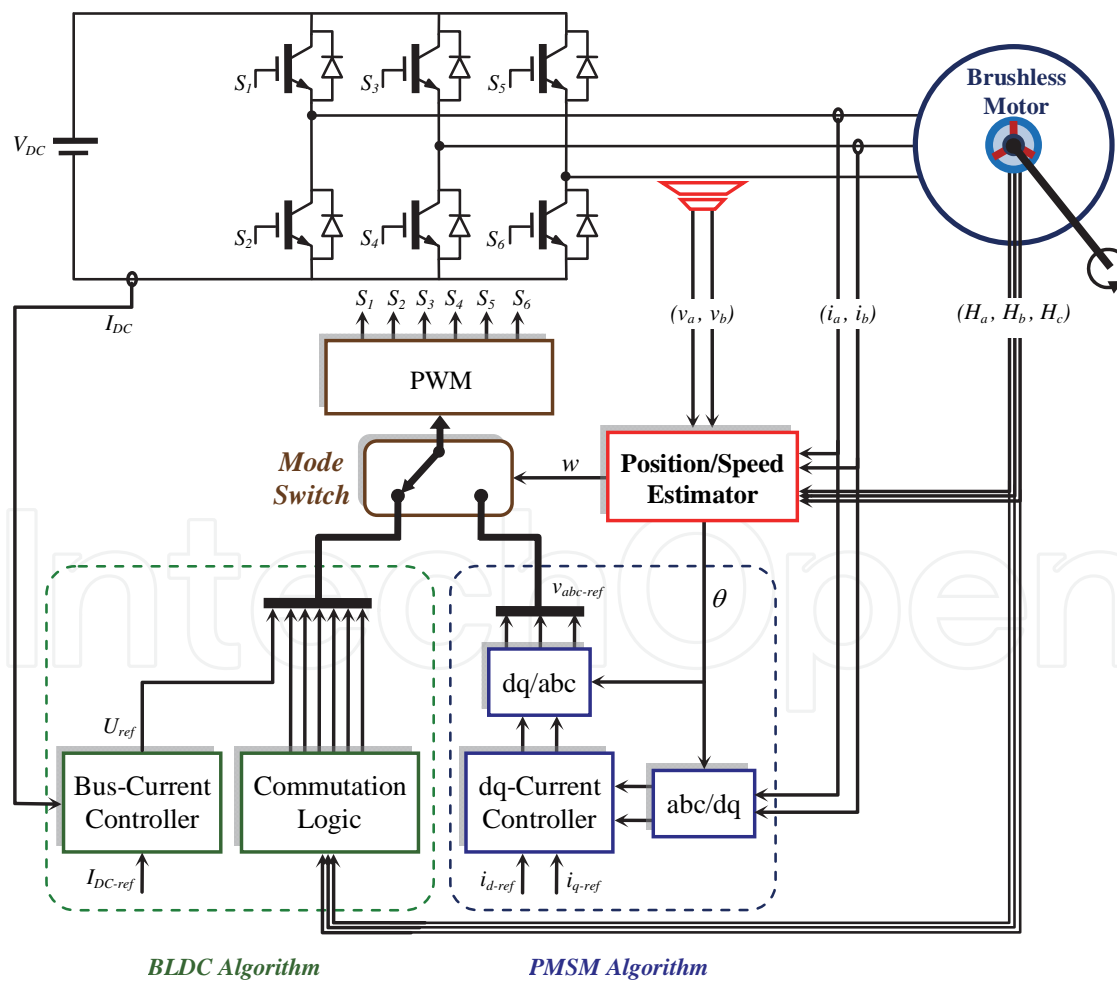


Fig. 9. Overall scheme of the combined BLDCM/Sensorless PMSM control strategy.

The three Hall-effect sensors are positioned in the machine stator in order to provide 60 electrical deg. resolution in rotor position sensing. Thus, the error on the rotor position estimation is reset every time the rotor magnetic axes enter a new 60° sector univocally identified by means of the three Hall-effect sensors stats as shown in Fig. 10. The position error $\Delta\theta$ is taken to be the angular difference at these special instants because no encoder is used in the drive.

To meet the low-speed/high-torque demand, which is crucial for effective EV traction systems, the three Hall-effect sensors are used to start up the motor in BLDC mode. Until the motor overcomes the vehicle inertia and the speed is high enough that mechanical quantities can be accurately estimated with the Back-EMF/Hall sensors estimation method, the operation algorithm is switched to the PMSM vector control mode.

Fig. 11 shows the curves of a-phase, d-q currents and torque as well as speed and position error at a transition moment from BLDC to PMSM operating mode. The motor runs at 50 rpm under 75% of the rated load in this test. The a-phase current wave-form reflects the six-step excitation mode, using only Hall-effect data, and the sensorless sinusoidal drive. The cancellation of the direct current i_d (black line) reflects the change to vector control with maximum torque strategy. Clearly, the generated torque and current are much smoother in PMSM control zone i.e. after 0.5s. That justifies the effectiveness of the technique in reducing power losses, noises and mechanical vibrations.

The position estimation error is delimited by a $\pm 10^\circ$ band but it is small on average. The speed estimate remains unaffected by the transition. Furthermore, it can be noticed especially during BLDC mode, that position error peaks appear six times per electrical period. They arise from the position refreshing at Hall-effect sensor edges.

The results given in Fig. 12 show successful starting up from standstill to 600rpm. The switching instant from BLDC to PMSM control mode is dictated by the speed when it reaches 50rpm (4 km/h). The speed threshold is chosen to have not only accurate estimation but also proper operation with considerable load. This speed value should be low and it is defined by tests. The transition behavior of the drive is highlighted by current and torque zoom. The technique provides an excellent mode transition and sensorless control with good position estimation ($\Delta\theta \leq 1^\circ$). Thanks to the BLDC mode, the motor can start with a very high torque that exceeds 200% of the rated torque. At the transition instant, the maximal rotor position error is around 15° which may generate 3.4% of torque loss. With this loss value, the sensorless PMSM drive keeps perfectly the ability to develop the large torque required to startup and maintain the motion. The motor current and torque, in the figure, exhibit the high efficiency and performance of the PMSM vector control, except for the first short interval.

The dynamic performances of the in-wheel motor drive are tested in an acceleration/deceleration speed profile from 200 rpm to 600 rpm (Fig. 13). The maximum continuous torque is about 80% of the rated load. The proposed position estimation works very reliably during such relatively severe conditions. The position error average is always very small (1°). The residual ripple is not usually a problem because it will be filtered out by the vehicle inertia.

The position error that arises from Hall sensors alignment defect, remains constant. So, it could be easily eliminated from the position estimate.

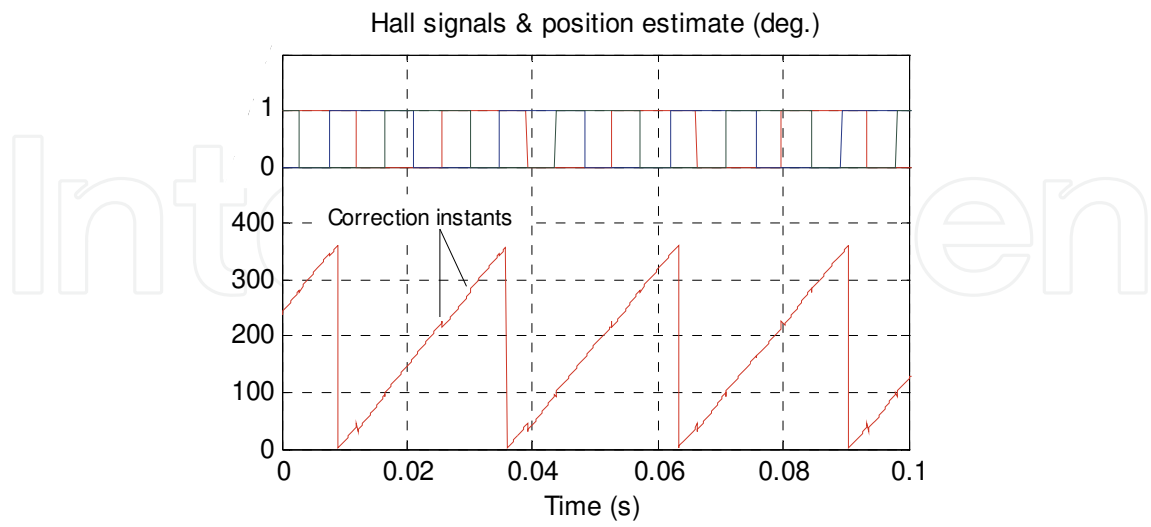


Fig. 10. Hall-effect signals and estimated position.

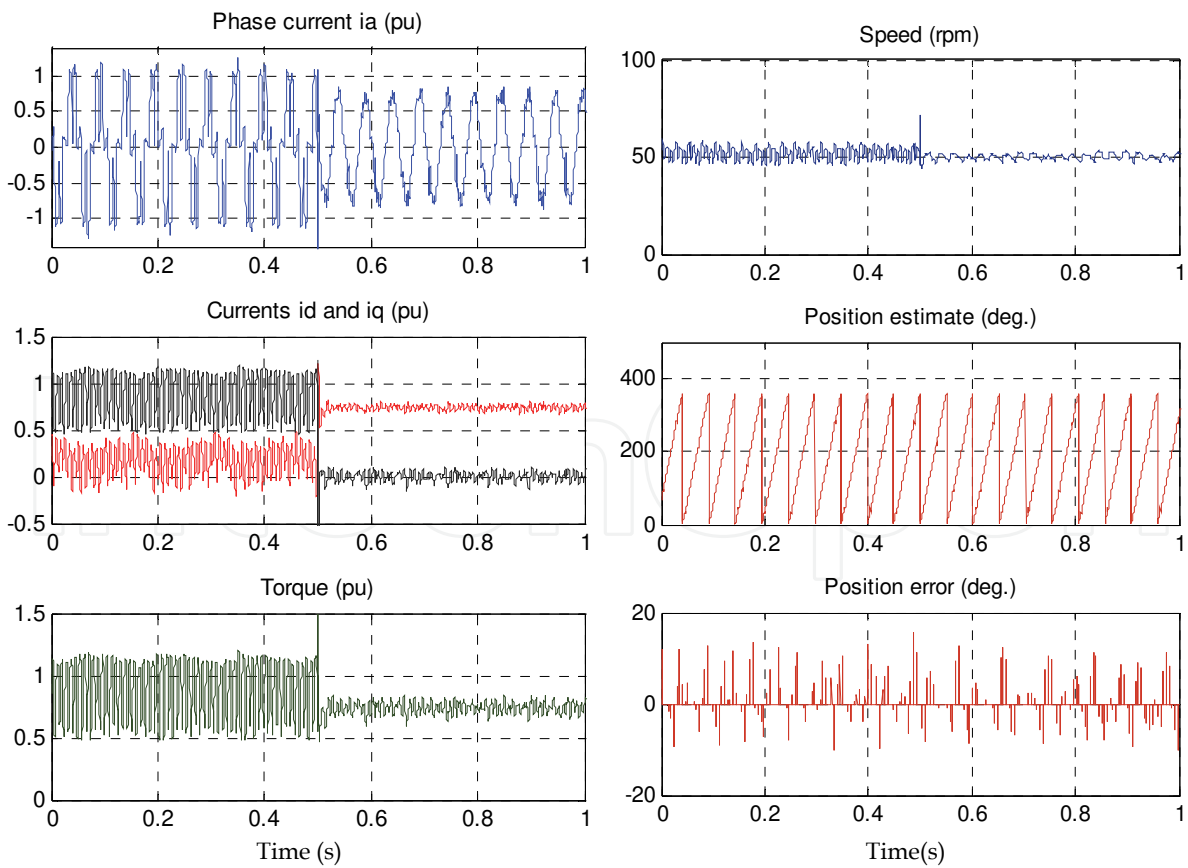


Fig. 11. Commutation from BLDCM mode to PMSM mode at 50 rpm.

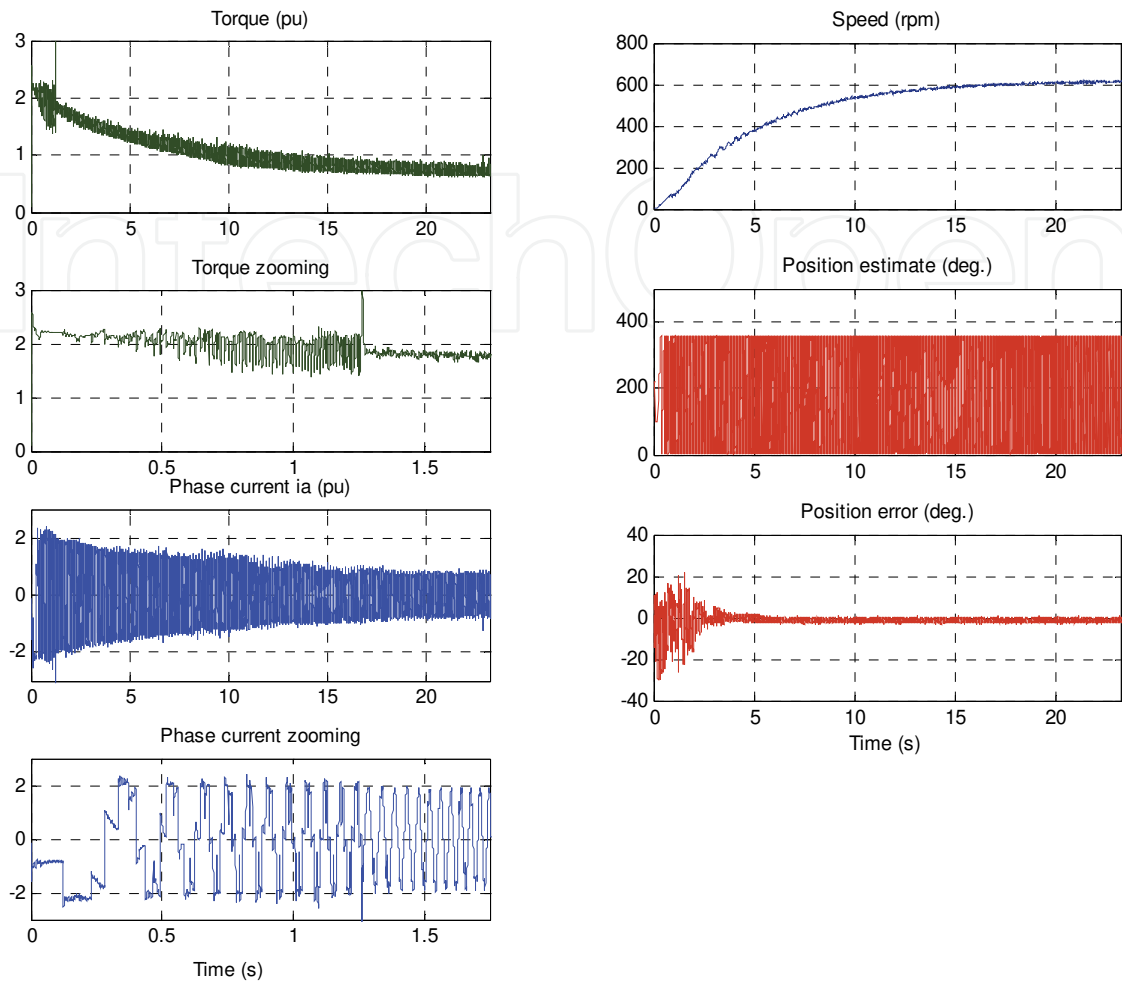


Fig. 12. Starting up with complete BLDCM/Sensorless PMSM control strategy.

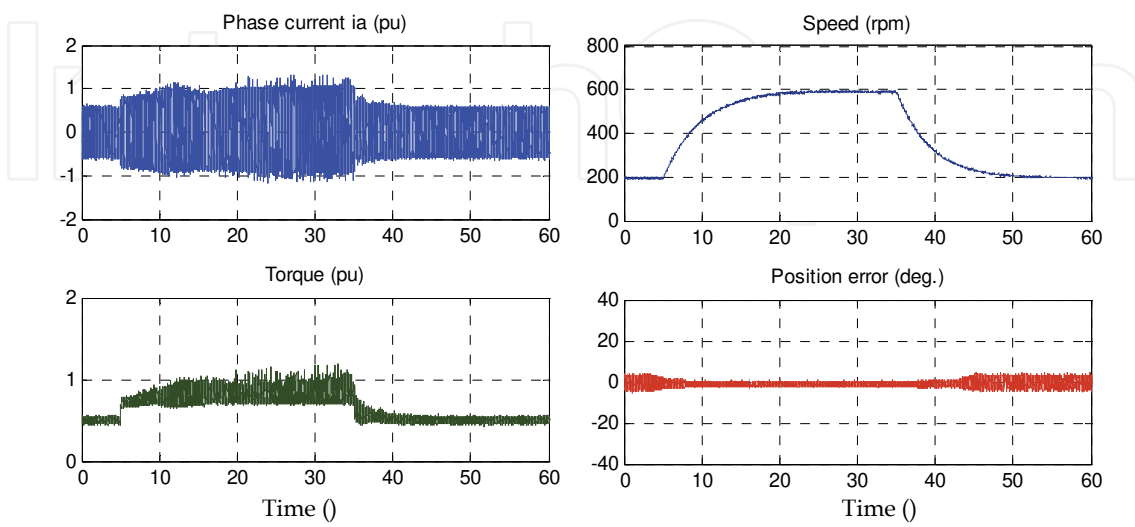


Fig. 13. Dynamic behavior of the drive in Sensorless PMSM control mode

6. Conclusion

The presented position and speed estimation technique is based on Hall-effect sensors and is dedicated to Electric Vehicle applications. The starting problem commonly encountered in such a field, is completely surmounted by using the Hall-effect pulses to start the machine as a BLDC Motor. Next, the Back-EMF based estimator in conjunction with Hall-effect sensors are used to achieve a very accurate estimation of the rotor position and speed for sensorless vector control of the motor in PMSM mode. That means the drive is not in need of special initial position detection or starting up technique.

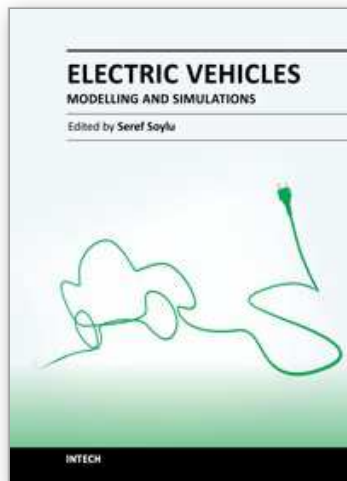
The experimental results show that the presented sensorless estimation algorithm provides high accuracy rotor position and speed. There are three major advantages associated with the proposed method:

- Minor sensitivity to the motor parameters and electrical measurement imperfections. The refreshment of the position estimation at every Hall signal edge, eliminates any position error whichever origin induces it.
- Extra-load starting up capability, as the Hall-effect sensors provides enough information for proper BLDC operation.
- Low computation time requirement and high reliability; the algorithm can be easily implemented by a microcontroller or DSP.

7. References

- Batzel, T.D. & Lee, K. Y. (2005). Electric Propulsion with the Sensorless Permanent Magnet Synchronous Motor: Model and Approach, *IEEE Transaction on Energy Conversion*, Vol. 20, No. 4, (December 2005), pp. 818-825.
- Capponi, F. G.; De Donato, G.; Del Ferraro, L.; Honorati, O.; Harke, M. C. & Lorenz, R. D. (2006). AC Brushless Drive With Low-Resolution Hall-Effect Sensors for Surface-Mounted PM Machines, *IEEE Transaction on Industry Applications*, Vol. 42, No. 2, (March/ April 2006), pp. 526-535.
- Capponi, G. ; De Donato, G. & Del Ferraro, L. (2004). Brushless AC Drive Using an Axial Flux Synchronous Motor with Low Resolution Position Sensors, *Proceeding of the IEEE 35th Annual Power Electronics Specialists Conference*, Vol. 3, pp. 2287-2292, Aachen, Germany, June 20-25, 2004.
- Carpaneto, M.; Maragliano, G.; Marchesoni, M. & Vaccaro, L. (2009). A New Sensorless Permanent Magnet Synchronous Motor Algorithm Based on Algebraic Method, *Proceeding of the 13th European Conference on Power Electronics and Applications*, pp. 1-10, Barcelona, Spain, September 8-10, 2009.
- Chau, K. T.; Chan, C. C. & Liu, C. (2008). Overview of Permanent-Magnet Brushless Drives for Electric and Hybrid Electric Vehicles, *IEEE Transaction on Industrial Electronics*, Vol. 55, No. 6, (June 2008), pp. 2246-2256.
- Chen, J.-L.; Liu, T.-H. & Chen, C.-L. (2010). Design and Implementation of a Novel High-Performance Sensorless Control System for Interior Permanent Magnet Synchronous Motors, *Electric Power Applications (IET)*, Vol. 4, No. 4, (April 2010), pp. 226-240.

- Cheng, K.-Y. & Tzou, Y.-Y. (2003). Design of a Sensorless Commutation IC for BLDC Motors, *IEEE Transaction on Power Electronics*, Vol. 18, No. 6, (November 2003), pp. 1365–1375.
- Emadi, A. (2005). *Handbook of Automotive Power Electronics and Motor Drives*, CRC Press-Taylor & Francis Group, ISBN: 0-8247-2361-9, USA.
- Genduso, F.; Miceli, R.; Rando, C. & Galluzzo, G. R. (2010). Back EMF Sensorless-Control Algorithm for High-Dynamic Performance PMSM, *IEEE Transaction on Industrial Electronics*, Vol. 57, No. 6, (June 2010), pp. 2092–2100.
- Gieras, J. F.; Rong-Jie Wang, R. J. & Kamper, M. J. (2004). *Axial Flux Permanent Magnet Brushless Machines*, Springer Science+Business Media B.V.-Kluwer Academic Publishers, ISBN: 1-4020-2661-7, Netherlands.
- Hanselman, D. C. (Second Edition, 2006). *Brushless Permanent Magnet Motor Design*, Magna Physics Publishing, ISBN: 1881855155, USA.
- Jain, M. & Williamson, S.S. (2009). Suitability Analysis of In-wheel Motor Direct Drives for Electric and Hybrid Electric Vehicles, *Proceeding of IEEE Electrical Power & Energy Conference*, pp 1-5, Montreal QC, Canada, October 22-23, 2009.
- Jingbo, L.; Nondahl, T.; Schmidt, P.; Royak, S. & Harbaugh, M. (2010). Equivalent EMF Based Position Observers for Sensorless Synchronous Machines, *Proceeding of the 25th Annual IEEE Applied Power Electronics Conference and Exposition*, pp. 425-432, Palm Springs, CA, February 21-25, 2010.
- Johnson, J. P.; Ehsani, M. & Guzelgunler, Y. (1999). Review of Sensorless Methods for Brushless DC, *Proceeding of IEEE Industry Application Society Annual Meeting*, Vol. 1, pp. 143–150, Phoenix, AZ, USA, October 3-7, 1999.
- Krishnan, R. (2010). *Permanent Magnet Synchronous and Brushless DC Motor Drives*, CRC Press-Taylor & Francis Group, ISBN: 978-0-8247-5384-9, USA.
- Morimoto, S.; Sanada, M. & Takeda, Y. (1996). Sinusoidal Current Drive System of Permanent Magnet Synchronous Motor with Low Resolution Position Sensor, *Proceeding of IEEE Industry Application Society Annual Meeting*, pp. 9-13, San Diego, CA, USA, October 6-10, 1996.
- Sungyoon, J.; Beomseok, L. & Kwanghee, N. (2010). PMSM Control Based on Edge Field Measurements by Hall Sensors, *Proceeding of the 25th Annual IEEE Applied Power Electronics Conference and Exposition*, pp. 2002-2006, Palm Springs, CA, USA, February 21-25, 2010.
- Yousfi, D. & El Adnani, M. (2007). PMSM Sensorless Control with Simple and Efficient Estimation Method, *Proceeding of the 7th International Conference on Power Electronics and Drive Systems*, Bangkok, Thailand, November 27-30, 2007.
- Yousfi, D. (2009). Encoderless PM Brushless Drive For Electric Vehicle Traction, *Proceeding of the 35th Annual Conference of the IEEE Industrial Electronics Society*, Porto, Portugal, November 3-5, 2009.
- Yousfi, D.; Ait Ouahman, A.; Elbacha A. & Boulghasoul Z. (2010). Combined BLDCM and Encoderless PMSM Control for Electric Hub Motor Drives, *Proceeding of the XIX International Conference on Electrical Machines*, Rome, Italy, September 6-8, 2010.



Electric Vehicles - Modelling and Simulations

Edited by Dr. Seref Soylu

ISBN 978-953-307-477-1

Hard cover, 466 pages

Publisher InTech

Published online 12, September, 2011

Published in print edition September, 2011

In this book, modeling and simulation of electric vehicles and their components have been emphasized chapter by chapter with valuable contribution of many researchers who work on both technical and regulatory sides of the field. Mathematical models for electrical vehicles and their components were introduced and merged together to make this book a guide for industry, academia and policy makers.

How to reference

In order to correctly reference this scholarly work, feel free to copy and paste the following:

Driss Yousfi, Abdelhadi Elbacha and Abdellah Ait Ouahman (2011). Efficient Sensorless PMSM Drive for Electric Vehicle Traction Systems, *Electric Vehicles - Modelling and Simulations*, Dr. Seref Soylu (Ed.), ISBN: 978-953-307-477-1, InTech, Available from: <http://www.intechopen.com/books/electric-vehicles-modelling-and-simulations/efficient-sensorless-pmsm-drive-for-electric-vehicle-traction-systems>

INTECH
open science | open minds

InTech Europe

University Campus STeP Ri
Slavka Krautzeka 83/A
51000 Rijeka, Croatia
Phone: +385 (51) 770 447
Fax: +385 (51) 686 166
www.intechopen.com

InTech China

Unit 405, Office Block, Hotel Equatorial Shanghai
No.65, Yan An Road (West), Shanghai, 200040, China
中国上海市延安西路65号上海国际贵都大饭店办公楼405单元
Phone: +86-21-62489820
Fax: +86-21-62489821

© 2011 The Author(s). Licensee IntechOpen. This chapter is distributed under the terms of the [Creative Commons Attribution-NonCommercial-ShareAlike-3.0 License](#), which permits use, distribution and reproduction for non-commercial purposes, provided the original is properly cited and derivative works building on this content are distributed under the same license.

IntechOpen

IntechOpen